

MACHINE BUILDING. PROCESS METALLURGY. MATERIALS SCIENCE

МАШИНОБУДУВАННЯ. ТЕХНОЛОГІЯ МЕТАЛІВ. МАТЕРІАЛОЗНАВСТВО

UDC 539.3

Ahmad Rahbar Ranji, PhD, Assoc. Prof.,
Amirhossein Kaviani,
Mehdi Iranmanesh, PhD, Assoc. Prof.,
Alireza Dowlatabadi

Department of Maritime Engineering, AmirKabir University of Technology, 424 Hafez Ave., Tehran, 15914, Iran, e-mail: rahbar@aut.ac.ir

EFFECT OF PITTING CORROSION ON STRESS INTENSITY FACTORS OF SEMI-ELLIPTICAL SURFACE CRACKS ON THE OUTER WALL SURFACE OF A TUBULAR T-JOINT

A. Рахбар Ранджі, А. Кавіані, М. Іранманеш, А. Довлатабаді. Вплив точкової корозії на коефіцієнти інтенсивності напружень напівеліптичних поверхневих тріщин на поверхні зовнішньої стінки трубчастого Т-подібного з'єднання. Втомна і точкова корозія є двома важливими конструктивними аспектами для оцінки міцності сталевих конструкцій морської нафтової і газової промисловості. Вкрай важливо оцінити вплив корозії на втомний термін служби пошкоджених сталевих конструкцій. Детальні дослідження тривалості поширення тріщин для втомних дефектів в трубопроводі та трубчастих з'єднаннях, відкритих до корозійного середовища, створюють серйозні проблеми для інженерної практики. Підхід лінійної пружної механіки руйнування (ЛПМР) можна використовувати для аналізу зростання високоциклової втомної тріщини, яка зазвичай виникає коли прикладені напруги значно нижче напруги текучості. У більшості випадків вважається, що коефіцієнт інтенсивності напружень (КІН) розраховується при аналізі і проектуванні структур із використанням ЛПМР. У даній роботі досліджено вплив точкової корозії на коефіцієнт інтенсивності напружень вздовж фронту тріщини. Дуже мало досліджень, які використовують метод кінцевих елементів (МКЕ) для оцінки коефіцієнта інтенсивності напружень вздовж фронту тріщини в Т-подібному з'єднанні із та без точкової корозії. Для того, щоб показати вплив ямки на параметр зламу, коефіцієнт піт-ефекту визначається як різниця між нормованими коефіцієнтами інтенсивності напружень із та без точкової корозії. В ANSYS відтворено серію тривимірних моделей кругових конусних ямок з напівеліптичною поверхневою тріщиною в трубчастому Т-образному з'єднанні. Для перевірки моделі результати непошкодженої моделі звірялися із наявними в літературі результатами та спостерігалися задовільні збіги. Проведено тривимірний кінцево-елементний аналіз з метою дослідити вплив глибини, орієнтації, площі поперечного перерізу і розташування точкової корозії. Таким чином проаналізовано ефекти геометрії і положення точкової корозії, а також розмір тріщини. Виявлено, що розташування і геометрія точкової корозії є домінуючими параметрами, що впливають на коефіцієнт інтенсивності напружень. Точкова корозія, розташована в напрямку поверхні тріщини і поблизу поверхневої тріщини, значно впливає на коефіцієнт інтенсивності напружень, тоді як виразкова корозія, розташована на трубі, що примикає, негативно впливає на КІН.

Ключові слова: точкова корозія, напівеліптична тріщина, метод кінцевих елементів, коефіцієнт інтенсивності напружень

A. Rahbar Ranji, A. Kaviani, M. Iranmanesh, A. Dowlatabadi. **Effect of pitting corrosion on stress intensity factors of semi-elliptical surface cracks on the outer wall surface of a tubular T-joint.** Fatigue and pitting corrosion are two important design considerations for strength assessment of steel structures of the offshore oil and gas industry. It is vital to evaluate the impact of corrosion on the fatigue life of corroded steel structures. Close examinations of the crack propagation life for fatigue-induced defects in the pipeline and tubular joint exposed to corrosion environment have posed serious challenges to engineering practice. The approach of linear elastic fracture mechanics (LEFM) can be used to analyze the growth of high-cycle fatigue crack, which typically occurs when the applied stresses are well below the yield stress. It is mostly accepted that the stress intensity factor (SIF) is calculated in the analysis and design of structures using LEFM. In the present study the effect of pitting corrosion on stress intensity factor along the crack front is investigated. Very few studies exist that employ the Finite element method (FEM) to estimate the stress intensity factor along the crack front in T-joint with and without pitting corrosion. In order to show the effect of pit on the fracture parameter, the pit-effect coefficient is defined as the difference between normalized stress intensity factors with and without pitting corrosion. A series of three-dimensional circular cone pit models together with a semi-elliptical surface crack in a tubular T-joint are simulated in ANSYS. In order to validate the model, the results of an un-corroded model are examined against the available results in the literature, and good agreements are observed. Three-dimensional finite element analyses are

DOI: 10.15276/opu.2.55.2018.01

© 2018 The Authors. This is an open access article under the CC BY license (<http://creativecommons.org/licenses/by/4.0/>).

conducted in order to investigate the effects of depth, orientation, cross-sectional area and location of pitting corrosion. Thus the effects of the geometry and position of pitting corrosion, as well as the size of crack, are being analyzed. It is found that the location and geometry of pitting corrosion are the dominant parameters affecting the stress intensity factor. The pitting corrosion located in the direction of crack face and close to the surface crack has a significant influence on the stress intensity factor, whereas the pitting corrosion located in brace has a negative effect on the SIF.

Keywords: Pitting corrosion, semi-elliptical crack, Finite element method, Stress intensity factor

Introduction. Fatigue failure of structures is a multidisciplinary phenomenon, which is still one of the main reasons for failures in structures, although advanced methods have been used in the design and manufacturing process. Offshore rigs and jackets are fabricated from tubular sections, in which the welded joints are the most highly stressed spots. Cyclic loads of wave, current, wind and quake lead to fatigue cracks in these joints, which can propagate to critical size. The approach of linear elastic fracture mechanics (LEFM) can be used to analyze the growth of high-cycle fatigue crack, which typically occurs when the applied stresses are well below the yield stress [1]. It is mostly accepted that the stress intensity factor (SIF) is calculated in the analysis and design of structures using LEFM.

Literature review and Formulation of the problem. A great number of studies and experiments with a variety of methods have assessed the fatigue life of T-joints [2 – 4]. Li et al. [5] analyzed the SIFs of a semi-elliptical surface crack located at the saddle point of welded tubular T-joints using the finite and boundary element methods by varying the brace thickness and weld size. They concluded that the inclusion of weld into the model did not influence the SIFs significantly. Similar results had already been reported by Huang and Hancock [6]. Huijskens [7] experimentally showed that fatigue cracks initiated from the weld toe on the chord close to the saddle point, and grew rapidly along the chord surface at the weld toe and deeply through the chord wall. Olowokere and Nwosu [8, 9] showed how the mode I linear elastic line spring elements were applied in conjunction with shell elements in a steel tubular T-joint containing a semi-elliptical surface crack. Many researchers examined SIFs along the surface crack front and measured the fatigue crack propagation based on fracture mechanics in a wide range of conditions [10 – 12]. Toribio et al. [10] evaluated the SIF at the surface crack front in round bars subjected to cyclic tension and bending. Qian et al. [11] analyzed the effects of crack front profile and the interaction between adjacent fatigue cracks on the fatigue driving force, by calculating SIFs using the finite element method (FEM).

Marine platforms, including ships and offshore structures are at high risk of corrosion. Aging also often leads to corrosion-induced deterioration of steel bridges, especially those on the coast or exposed to de-icing salts, high humidity and moisture. Corrosion is generally divided into two types, i.e. general corrosion and localized corrosion. Pitting corrosion is categorized as one form of localized corrosion. There exists very rich literature in this area, particularly about the structural strength of plates with corrosion pits in multiple aspects. Examples include studies on the effects of corrosion pits on buckling of plates [13], prediction of stress concentration factor of corrosion pits on pipes [14], ultimate strength of stiffened plates with pitting corrosion [15], and blast strength of corrosion plates [16 – 18].

Corrosion and fatigue have been recognized as significant and major damage mechanisms for marine structures [19]. It is vital to evaluate the impact of corrosion on the fatigue life of corroded steel structures. Close examinations of the crack propagation life for fatigue-induced defects in the pipeline and tubular joint exposed to corrosion environment have posed serious challenges to engineering practice [20]. In general, the vast majority of research on the influence of pitting corrosion on crack has been focused on pitting leading to fatigue crack initiation and crack growth or pitting nucleation, pit growth, the transition from pitting to fatigue crack initiation, short crack growth, and long crack growth [21, 22]. Wang et al. proposed a 3D geometric model for pitting corrosion and employed a three dimensional FEM to determine the SIF for pitting corrosion with various geometric properties [23]. Pit configuration has been at the center of a controversy in maritime engineering. Based on the experimental observations on two types of ships with different ages, Nakai [24] reported that the shapes of the corrosion pits were circular cones, with the ratio of diameter to depth being in the ranges of 8 to 1, and 10 to 1, respectively, and the diameters being approximately smaller than 10 mm. Eventually, Jie et al. demonstrated that fatigue cracks do not necessarily initiate at the edge or bottom of pits, and other causes, such as weld toe, definitely exert influences on the location of crack initiation [25]. When pit and

crack are a distance from each other, the effects of shape, dimensions of pits and the distance between them have not been examined yet in the aforementioned studies individually.

Purpose of the study. In the present research of a tubular T-joint the effect of cone pits on the SIF is studied. Different values of depth, orientation, area of cross-section, and pit location are investigated by conducting a series of three-dimensional finite element analyses using the ANSYS code.

Finite element analysis. FEM is one of the most common, powerful and flexible tools in rational structural analysis, which makes it possible to predict the strength of complex structures more accurately than existing classical theoretical methods. Fig. 1 shows the typical geometry of a T-joint and crack site. The surface crack is semi-elliptical, with semi-major axis “ c ” and semi-minor axis “ a ” (Fig. 2). The geometry of such a crack can be described by two dimensionless parameters, $\alpha=a/c$ and $\varepsilon=a/T$, called the aspect ratio and relative depth of crack, respectively, in which T is a symbol of chord thickness. To determine the position of a point on the semi-elliptical crack front, the relative location is defined as the ratio of arc length measured from the corner of the crack to the point under consideration, ξ , over the total length of crack front, h .

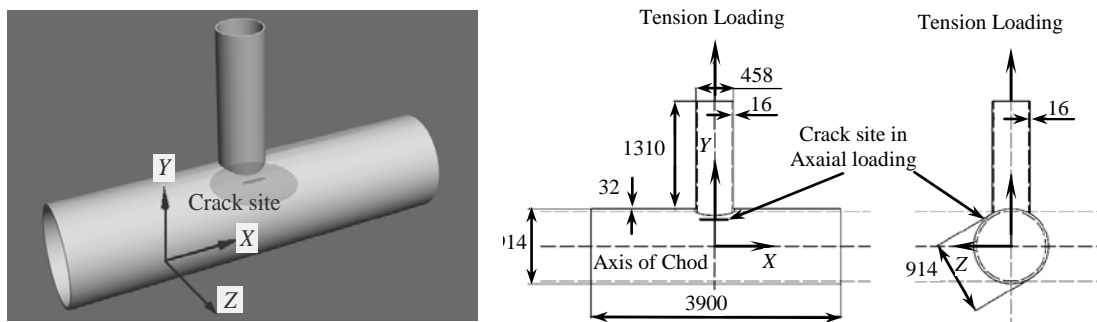


Fig. 1. Geometry of a common T-joint and position of a surface crack (the dimensions shown are in millimeter)

In order to investigate the effect of pit corrosion on SIF, the tubular T-joint (Fig. 1) taken from Lie et al. [5] is considered. It is assumed that the joint is axially loaded with a force of 925 kN in the y-direction and the two ends of the chord are rigidly restrained in all directions. Yield stress, Poisson’s ratio and Young’s modulus are taken as 250 MPa, 0.3, and 200 GPa, respectively.

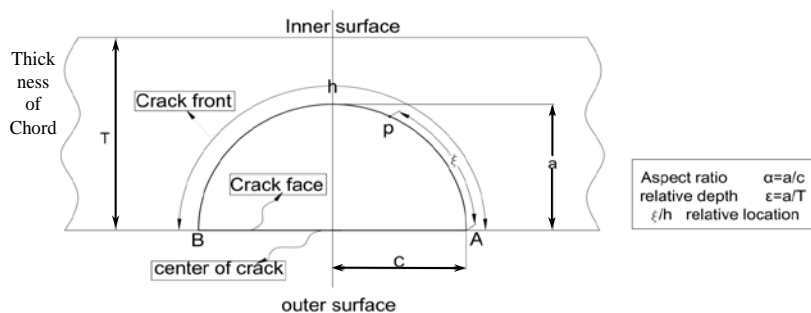


Fig. 2. Schematic illustration of a semi-elliptical surface crack

The geometry of this T-joint is generated in ANSYS; and the SOLID-187 element, which is a tetrahedral structural solid element with 10 nodes (mid-side nodes) and three degrees of freedom per node, is used to mesh it, except for the region around the crack tip. This region is meshed with the SOLID 186 element, a three-dimensional one with 20 nodes, exhibiting quadratic displacement behavior. The SIF is computed along the crack front using the interaction integral method. In order to meet the computational requirement, the entire structure is divided into several different zones as refined mesh zones, coarse zones, and transition zones (Fig. 3). The refined mesh zones are used around the crack and pitting corrosion (Figs. 4a and 4b). The coarse zones which are associated with the regions far from the joint have a negligible impact on the SIF. The transition zones connect these two types of zones together.

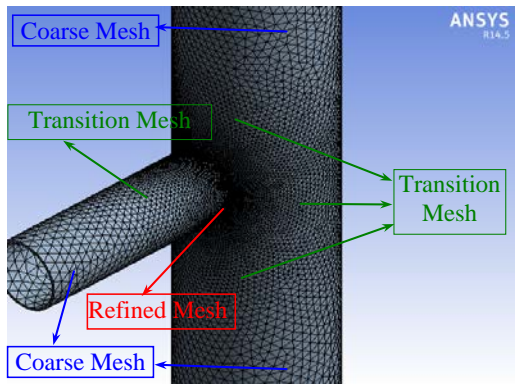


Fig. 3. The finite element mesh for tubular T-joint

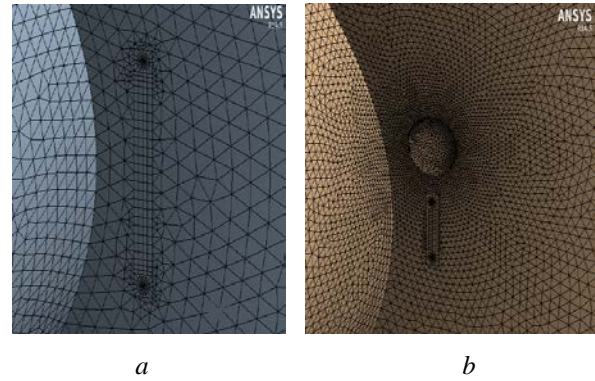


Fig. 4. Mesh generation for the crack (a), Refined mesh zone used around the crack and the pitting corrosion (b)

Mesh sensitivity analysis and verification of FEM. The size of mesh is a crucial factor influencing accuracy and computational efficiency. In order to determine the best mesh size, a sensitivity analysis is carried out for the T-joint of Fig. 1. Five pilot models including the cases of small semi-elliptical surface cracks and large ones are considered. For small cracks the maximum SIF occurs at the deepest point and the half-length of crack is greater than the depth of crack; whereas for large cracks it is the other way around. Figs. 5a and 5b give the results of five analyses for small and large cracks, respectively. As can be seen, when the number of mesh increases nine times from around 60000 to 500000, the SIF only increases by around 1%. Therefore, the size of mesh is chosen as 152346 elements for small cracks, and 125671 elements for large cracks, respectively, which show good accuracy with reasonable computational efficiency.

In order to verify the accuracy of FEM some numerical and experimental studies available in the literature have been revisited. Fig. 6 shows the comparison between the SIFs at the deepest point of the crack front calculated using the 3D FEM and those from Lie et al. [5]. As can be seen, there is very good agreement between the results of the present study and the available experimental and numerical ones. The maximum difference between the results of the three-dimensional FEM and those presented by Lie et al. [5] is about 5.5% for the case of $a=24$ mm.

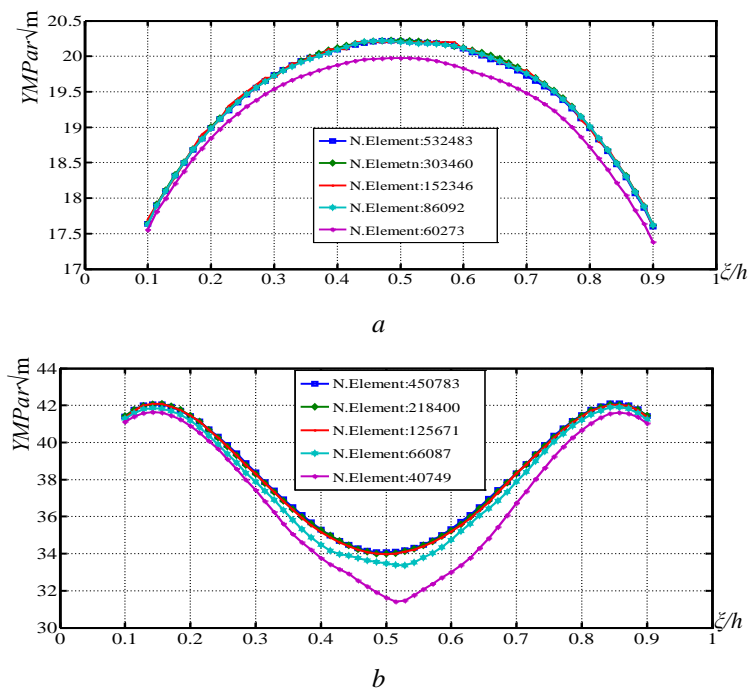


Fig. 5 Distribution of normalized SIF along the crack front:
Small crack ($c=15.1$ mm, $a=6.5$ mm) (a),
Large crack ($c=24.2$ mm, $a=101.1$ mm) (b)

Results and discussion. The calculation of SIF along the semi-elliptical crack front in this study is based on the following three assumptions:

1. T-joint is made of a homogenous, isotropic and linear elastic material.
2. The crack is of mode I.
3. There is no intersection between the pits and the crack.

To show the influence of pits on the SIF, a coefficient named pit effect is defined as:

$$\text{“Pit effect”} = \frac{Y_p^* - Y^*}{Y^*} \times 100, \quad (1)$$

where Y_p^* and Y^* are normalized SIFs with and without pitting corrosion, respectively. In this study, three different positions for pits are considered, i.e., pits in the direction of crack face, below the crack, and on the brace. The dimensions of circular pit are determined by two parameters: radius of the cross-sectional area of pit, r , and depth of pit, d . Table 1 shows the geometric characteristics of the considered cases.

Table 1

Geometric characteristics of considered crack and pits with $\varepsilon=0.2$, $r=20$ mm and $d=10$ mm

Number of pits	Location of pit(s)	Crack parameter
One pit on the chord	in the direction of crack face (Fig. 7)	$\alpha=0.4, 0.6, 0.8, 1.0, 1.2$
	below the crack (Fig. 9)	$\alpha=0.6$
One pit on the brace	vertical position (Fig. 13a)	$\alpha=0.4$
	circumferential position (Fig. 13b)	
Multi-pit along the crack	on each side of the crack (Fig. 15a)	$\alpha=0.4$
	on one side of the crack (Fig. 15b)	

One pit on the chord. In the first place, the effect of pits located in the direction of crack face is investigated (Fig. 7). Fig. 8 shows the SIF distributions along the crack front when pits are in the direction of crack face with different values of α . As can be seen, the effect of pit on SIF distribution becomes more dominant when pit gets closer to the center of surface crack. The increase of SIF is more prominent on the inner side than on the outer side. For example, for the case of $x=48$ mm, $\alpha=0.2$ and $\varepsilon=0.4$, the pit effect is around 10 % at the inner surface point, $\xi/h=0.1$, and 4 % at the outer surface point, $\xi/h=0.9$. It should be noted that pit effect decreases gradually with the increase of distance between the pit and the center of crack. The SIF distribution along the crack front decreases gradually until the effect of pit completely becomes nil.

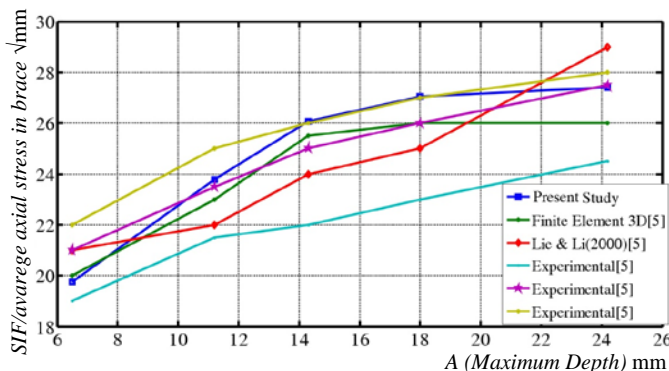


Fig. 6. Distribution of SIF at surface cracks in a tubular T-joint for different values of crack depth

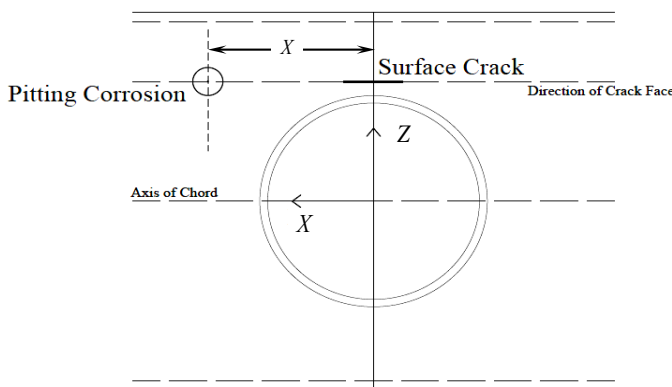


Fig. 7. Definition of pit located in the direction of crack face on the chord (x)

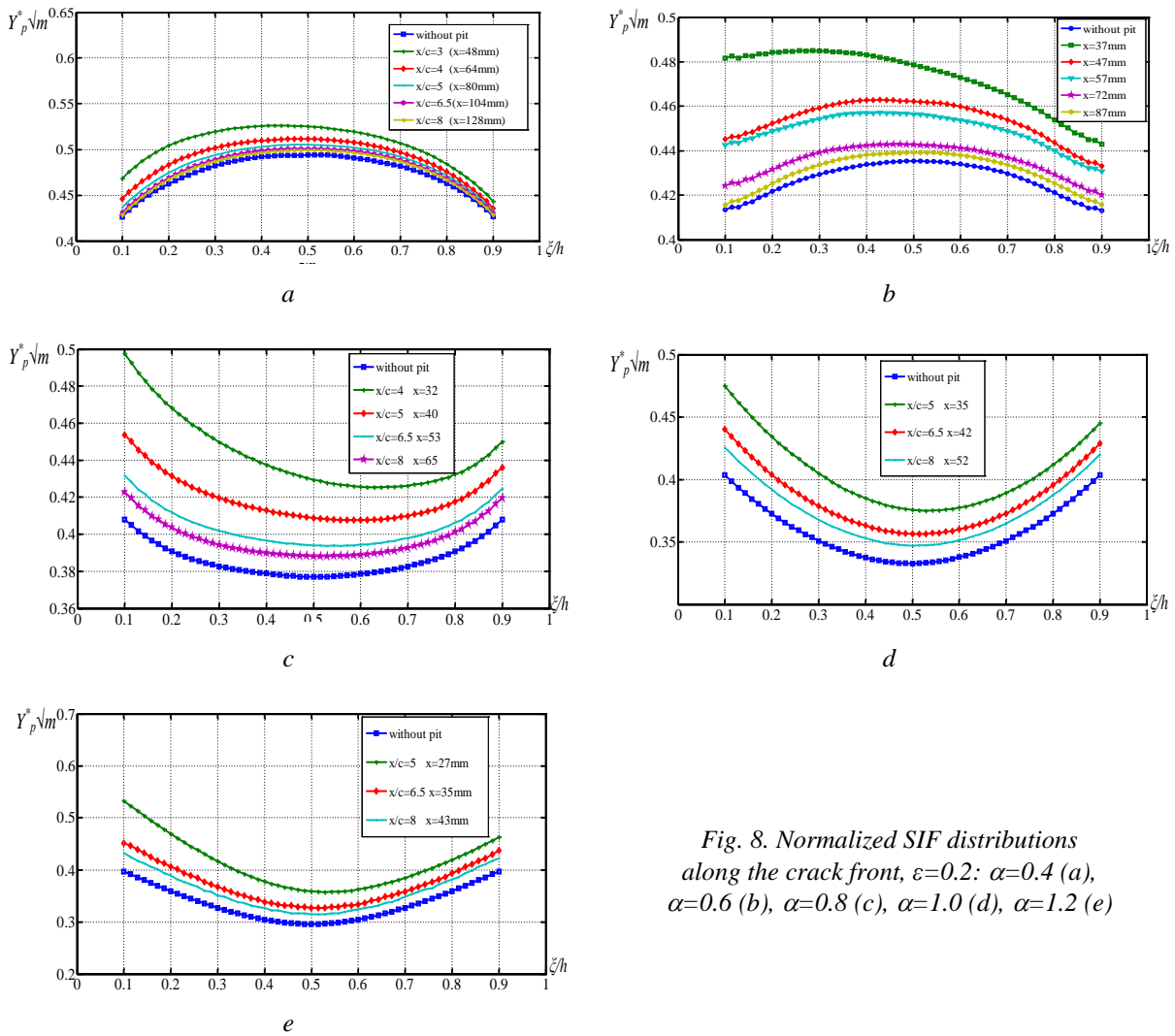


Fig. 8. Normalized SIF distributions along the crack front, $\varepsilon=0.2$: $\alpha=0.4$ (a), $\alpha=0.6$ (b), $\alpha=0.8$ (c), $\alpha=1.0$ (d), $\alpha=1.2$ (e)

When the pit is below the crack on the chord, two parameters are used to define its position with respect to the crack, i.e., the angle between the pit and the center of crack, ρ , as shown in Fig. 9, and the horizontal distance between them, x .

Fig. 10 demonstrates the effect of pitting corrosion for different angles ρ when $x=0$. This group of pits leads to symmetric reductions of SIF along the crack front. In other words, the presence of pit below the crack on the chord increases the fracture toughness of a cracked T-joint. It is observed that as the pit gets closer to the crack, the pit effect increases sharply. When $\rho=4^\circ$ and $\rho=6^\circ$, the pit effects are -12% and -3% , respectively, along the crack front; and when $\rho=8^\circ$, the pit effect reduces to only -1% , which results from the insignificant effect of pitting corrosion on the SIF.

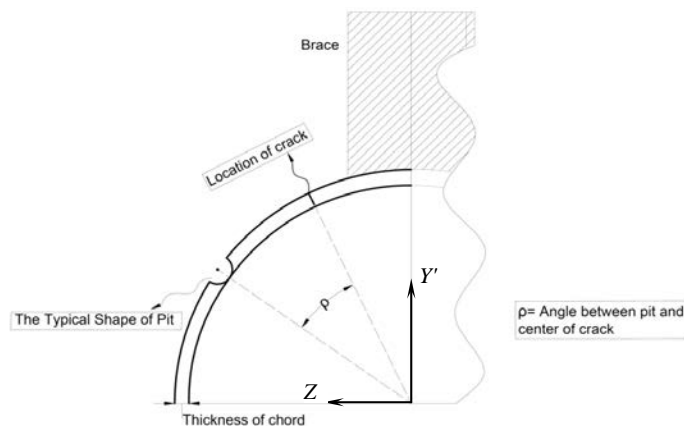


Fig. 9. Definition of angle between the pit and the center of crack (ρ)

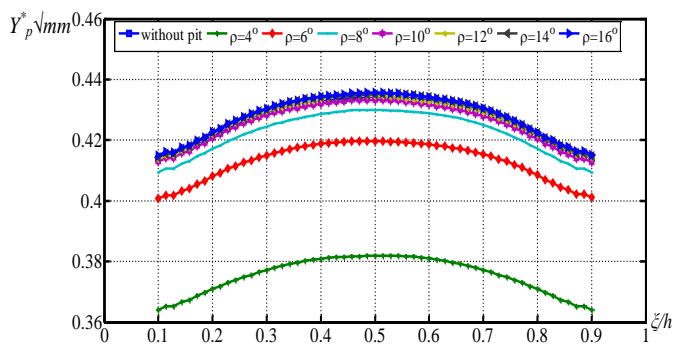


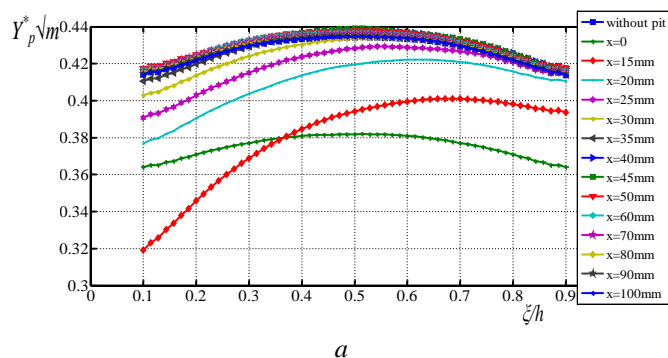
Fig. 10. Normalized SIF distributions along the crack front for different angles (ρ), $x=0$

around -23% and -6% , respectively, at the inner surface point, $\xi/h=0.1$, and around -5% and -3% , respectively, at the outer surface point, $\xi/h=0.9$; while when $x=0$, the pit effects are regularly -12% and -3% , respectively, along the crack front for the same angle (ρ). In these two cases, at $\xi/h=0.1$, the pit effects for $x=15\text{ mm}$ are both twice as high as those for $x=0$; where as at $\xi/h=0.9$, the pit effect becomes smaller from $x=0$ to $x=15\text{ mm}$ for $\rho=4^\circ$, but keeps the same for $\rho=6^\circ$. Except for $0 \leq x \leq 15\text{ mm}$, the effect of pit decreases as x increases at each point along the crack front.

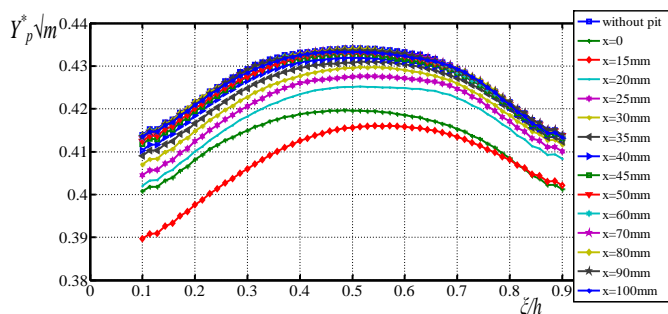
Figs. 12a, 12b, and 12c show the effect of pitting corrosion below the crack face at three points (i.e., the inner surface, the deepest and the outer surface points) for different distances between the pitting corrosion and the center of the crack (x). Based on the results presented in Fig. 12 for three relative locations of surface crack ($\xi/h=0.1$, $\xi/h=0.5$ and $\xi/h=0.9$), the effect of pitting corrosion should be divided into two phases termed A and B (Fig. 12). (If the SIF is calculated without pitting corrosion, the normalized SIF will be around 0.41 at the inner and outer surface points, and around 0.42 at the deepest point for the semi-elliptical crack mentioned in Table 1). It is shown that pits initially cause the SIF to decrease. Therefore, the value of pit effect is negative in phase A, which is followed by phase B, where the effect of pit on SIF becomes nil. With the increase of the distance between the pitting corrosion and the center of crack (x), the pit increases the SIF along the crack front even though the value of pit effect is small (around $+1\%$). As expected, pitting corrosion ultimately has an insignificant impact on the SIF and the pit effect approaches zero again.

One pit on the brace. To analyze the effect of pits (Table 1) on the brace on the SIFs along the crack front, two groups of pitting corrosion are considered. One is the vertical position of pits on the brace (Y), where pits are located in both directions of the brace axis and at the center of

Figs. 11a and 11b illustrate the normalized SIF distributions influenced by pitting corrosion for various distances between the pitting corrosion and the center of crack (x) at $\rho=4^\circ$ and $\rho=6^\circ$, respectively. When the pitting corrosion is not aligned with the center of crack ($x \neq 0$), the SIF patterns become asymmetric along the crack front (Fig. 11) and the effect of pitting corrosion at the inner surface is greater than that at the outer surface. When a pit is a short distance from the crack ($0 \leq x \leq 15\text{ mm}$), the effect of pit differs at each angle (ρ). When $x=15\text{ mm}$, for the cases of $\rho=4^\circ$ and $\rho=6^\circ$, the pit effects are



a



b

Fig. 11. Normalized stress intensity factor along the crack front when the pit is below the crack at a horizontal distance of x , at $\rho=4^\circ$ (a), at $\rho=6^\circ$ (b)

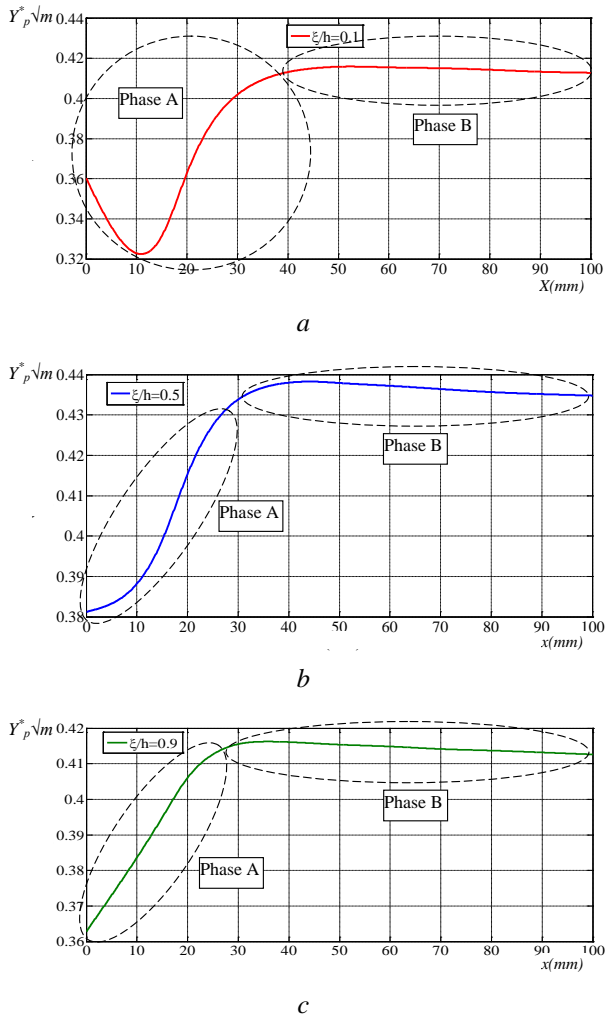


Fig. 12. Normalized stress intensity factor along the crack front with the pit below the crack at angle $\rho=4^\circ$, with different horizontal distances (x), for $\xi/h=0.1$ (a), for $\xi/h=0.5$ (b), for $\xi/h=0.9$ (c)

the crack (Fig. 13a); the other is the circumferential position of pitting corrosion on the brace (φ) (Fig. 13b). It is observed that all pits placed on the brace decrease the SIFs along the crack front, and the pit effect reaches the peak value of around -5% at $Y=417$ mm. When the vertical position (Y) of pit decreases, the effect of pit increases symmetrically (Fig. 14a). However, the pits located in the circumferential position decrease the SIF along the crack front asymmetrically (Fig. 14b). For example, when $Y=447$ mm and $\varphi=5^\circ$, the pit effects are -2% and -1% at the inner surface point, $\xi/h=0.1$, and the outer surface point, $\xi/h=0.9$, respectively. It should be noted that while the circumferential position of pitting corrosion increases from 0° to 25° , the trend of the effect of pit on the SIF changes differently. Between 0° and 10° the effect of pit increases, especially at the inner surface point. When $\varphi > 10^\circ$, the effect of pit begins to decrease and eventually reaches zero. Therefore, at $\varphi=20^\circ$ and $\varphi=25^\circ$ pitting corrosion has no influence on the SIF along the crack front (Fig. 14b).

Multi-pit along the crack face. Two types of situations are considered in this study (Table 1). The first one is that there is one pit on each side of the crack (Fig. 15a); the other is that pits are only located on one side of the crack (Fig. 15b). In these figures, x is the distance between the pit and the center of crack, and P is the distance between adjacent pits.

When there is one pit on each side of the crack, the pit effect at any surface point along the crack front can be calculated by algebraically adding the effect of a single pit at that surface point and that at the corresponding surface point on the other side of the crack (Fig. 16a). For example, when $x=48$ mm, it is observed that the pit effect at $\xi/h=0.1$ is around 14% . When a single pit is in the right hand of the

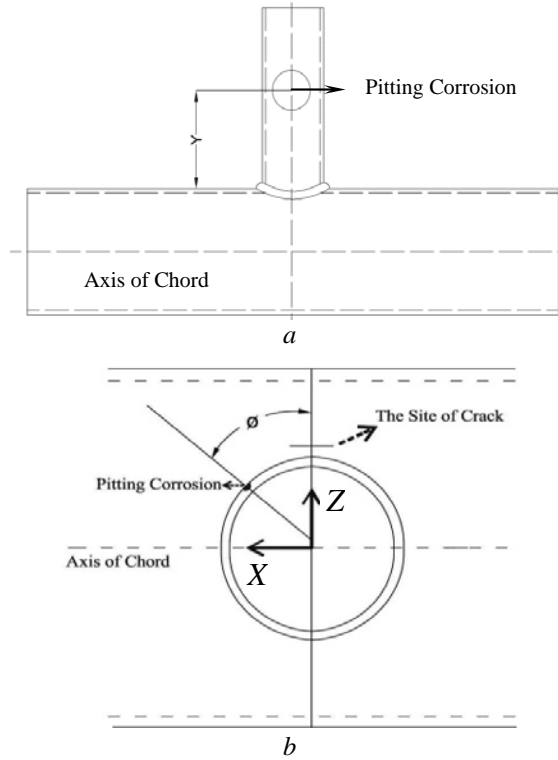


Fig. 13. Definition of pit located on the brace, a) vertical position of pit (Y), b) circumferential position of pit (φ)

crack, the pit effect is around 10 % at the inner surface point ($\xi/h=0.1$) and around 4 % at the outer surface point ($\xi/h=0.9$). It is thus concluded that the pit effect of 14 % at $\xi/h=0.1$ is obtained by algebraically adding the pit effect of 10 % at $\xi/h=0.1$ and that of 4 % at the corresponding surface point of $\xi/h=0.9$.

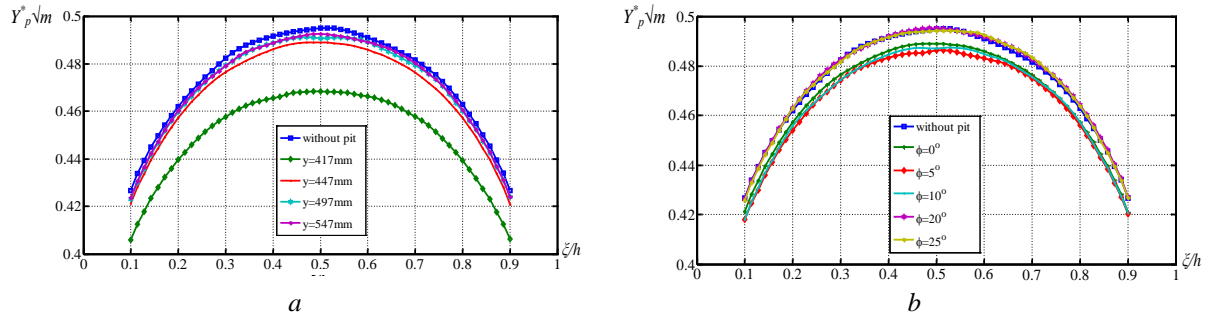


Fig. 14. Normalized stress intensity factor along the crack front for various a) vertical positions of pits on the brace, b) circumferential positions of pits on the brace when $Y=447$ mm

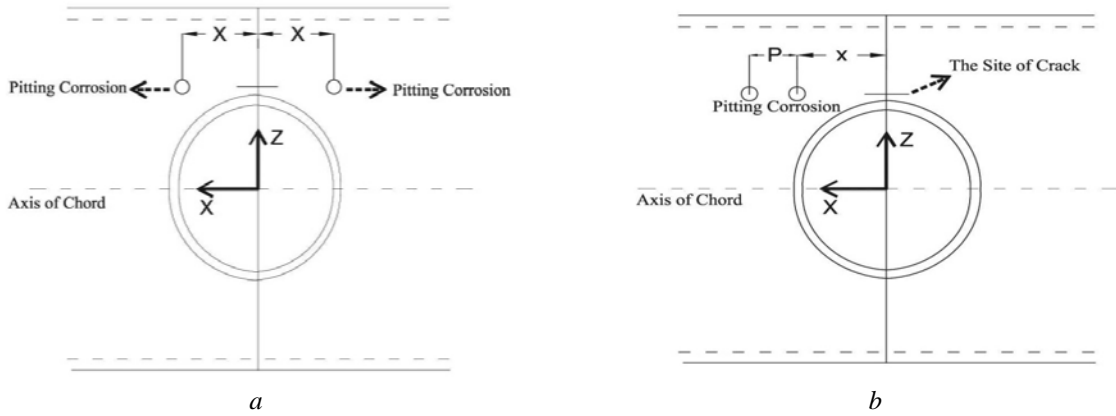


Fig. 15. Two types of models considered when analyzing the effect of multi-pit along the crack face: one pit on each side of the crack (a), pits only on one side of the crack (b)

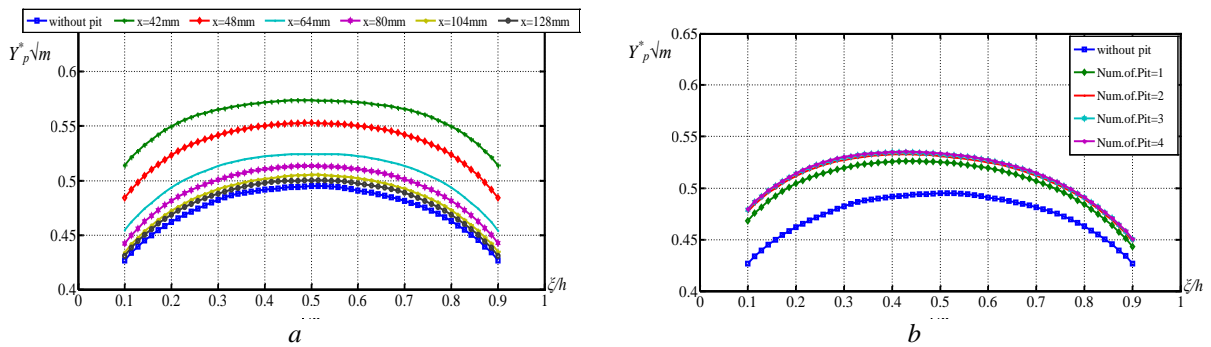


Fig. 16. Normalized stress intensity factor along the crack: one pit located on each side of the crack with different distances (a), pits located on one side of the crack (b)

The effect of the pits located only on one side of the crack behaves similarly to that of one pit on each side of the crack. The difference is that the pit effect in this case is determined by algebraically

adding the effects of each pit at the same point along the crack front. The results are illustrated in Fig. 16b. Four analyses are conducted as follows:

Analysis 1: one pit, which distance from the center of the crack is $x=48$ mm.

Analysis 2: two pits, which distances from the center of the crack are $x=48$ mm and $x=98$ mm, respectively.

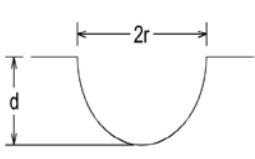
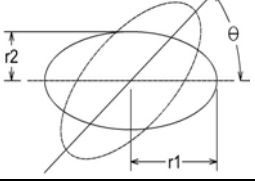
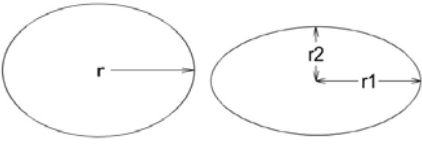
Analysis 3: three pits, which distances from the center of the crack are $x=48$ mm, $x=98$ mm and $x=148$ mm, respectively.

Analysis 4: four pits, which distances from the center of the crack are $x=48$ mm, $x=98$ mm, $x=148$ mm and $x=198$ mm, respectively.

So far the effect of different locations of pitting corrosion on the SIF has been investigated in this paper. Because of their significant positive pit effects, the pits located in the direction of crack face are used to analyze the effects of geometrical parameters of pitting corrosion on the SIF. The pit specifications are tabulated in Table 2 in order to study the effects of orientation, depth and area of pitting corrosion on the SIF. For each analysis the dimensionless parameters of semi-elliptical surface crack that remain constant are $\alpha=0.6$ and $\varepsilon=0.2$.

Table 2

Shapes of the corrosion pits for analyzing the effects of geometrical parameters of pitting corrosion on the SIF

	Kind of analysis		
	Effect of pit depth	Effect of pit orientation	Effect of pit area
Pit shape			
Variable parameter	$d(\text{mm})=5, 10, 20, 30$	$\theta^\circ=0, 20, 40, 60, 80, 90$	Circular area: $A0(\text{mm}^2)=314.159, 962.113, 1256.637$ Elliptical area: [$r1(\text{mm})=20, r2(\text{mm})=10$]
Constant parameters	$r=10$ mm $A0(\text{mm}^2)=314.159$ $x(\text{mm})=48$	$r1(\text{mm})=20$ $r2(\text{mm})=10$ $d(\text{mm})=20$ $x(\text{mm})=48$	$d(\text{mm})=20$ $x(\text{mm})=48$

Depth of pitting corrosion. Fig. 17 shows the effect of pit depth on the SIF along the crack front. The dimensions of pits are tabulated in Table 2. The effect of pit on the SIF increases symmetrically along the crack front as the depth of pit increases, but when the depth of pit is greater than $d=20$ mm, the pit effect becomes stable.

Orientation of pitting corrosion. Finite element analyses are performed to determine the effect of pit orientation on the SIF by using six different directions from 0° to 90° (Table 2). Fig. 18 shows that for different values of the pit angle θ , the normalized SIF along the crack front is a function of the relative location. It is observed that, in general, the pit effect decreases with the increase of θ , e.g., it is similar for each point along the crack front that the pit effects at $\theta=20^\circ$ are almost twice as much as those at $\theta=60^\circ$. The comparison between $\theta=60^\circ$ and $\theta=90^\circ$ shows the magnitude of differences of around 1 % along the crack front, which means that the effect of pit at $\theta=60^\circ$ is not significantly different from that at $\theta=90^\circ$.

Area of pitting corrosion. For each crack (Table 2) the normalized SIF shows an increasing trend with the area of cross-section; the effects of pits with cross-sectional areas of 314.159 mm^2 , 962.113 mm^2 and 1256.637 mm^2 on the SIF at the deepest point of crack are approximately 3 %, 8 % and 12 %, respectively (Fig. 19). It should be noted that the cross-sectional area of a circular pit

($A_0=962.113 \text{ mm}^2$), which radius is 17.5 mm, is higher than that of an elliptical pit ($A_0=628.318 \text{ mm}^2$), which major and minor radii are 20 mm and 10 mm, respectively. In spite of this fact, the effect of pit with a circular cross-section is smaller than that with an elliptical cross-section. The comparison of pit effect between the cases of circular cross-section and elliptical cross-section shows that, although the cross-sectional area of an elliptical pit is smaller than that of a circular pit, the pit effect of the former is greater than that of the latter because the radius, which is in the direction of the crack front, has a considerable effect on the SIF. In other words, for an elliptical pit, its cross-sectional area and radius (which is especially in the direction of the crack front) both affect the SIF.

Conclusions. Very few studies exist that employ the FEM to estimate the stress intensity factor along the crack front in T-joint with and without pitting corrosion. In order to show the effect of pit on the fracture parameter, the pit-effect coefficient is defined as the difference between normalized stress intensity factors with and without pitting corrosion. A series of three-dimensional finite element analyses are conducted in ANSYS to investigate the effects of depth, orientation, cross-sectional area and location of pitting corrosion. Based on the results obtained in this study the following conclusions are drawn:

- Two groups of pitting corrosion significantly increase the stress intensity factor along certain crack front in a T-joint, and the increment depends on both the shape of pitting corrosion and the distance between the pit and the center of crack. Pits of the first group are located in the direction of the crack front. Pits of the second group are located below, but sufficiently far from the crack, which have an insignificant effect (i.e. no higher than 1 %) on the SIF. Other than these two groups of pits other pits either reduce the SIF if they are close to the crack, or have no effect on the SIF.
- In the multi-pit state pits are located either on both sides of the crack or on one side of the crack. In order to calculate the effect of one pit on each side of the crack, the pit-effect coefficient at any surface point along the crack front is calculated by algebraically adding the pit-effect coefficients of a single pit at that surface point and at the corresponding surface point on the other side of the crack. Moreover, for pits located only on one side of the crack the pit-effect coefficient of all pits at some specific point can be calculated by algebraically adding the pit-effect coefficient of each pit at this point along the crack front.
- With the increase of the pit depth the effect of pitting corrosion increases to some certain value and then remains unchanged. However, this process mainly depends on the location of pit. Taking the pit located at $x=48 \text{ mm}$ for example, the effect of pitting corrosion reaches its maximum when $d=20 \text{ mm}$.

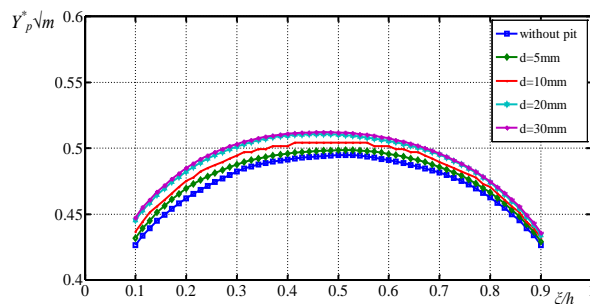


Fig. 17. Normalized stress intensity factor along the crack with different values of pit depth

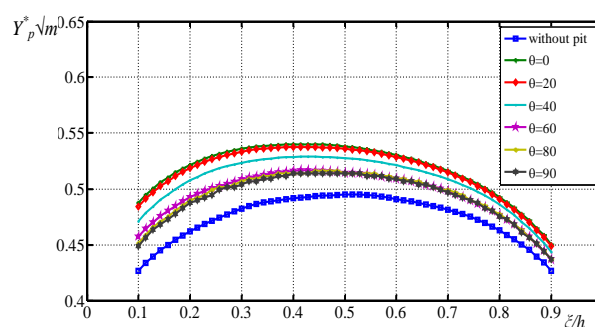


Fig. 18. Normalized stress intensity factor along the crack with different orientations of pit

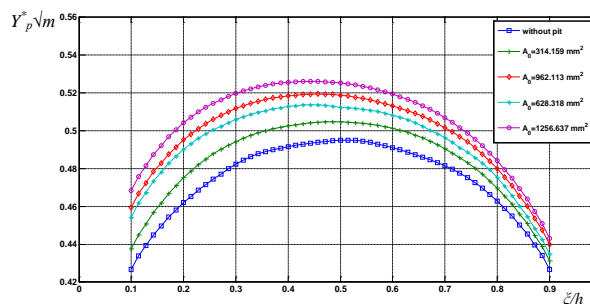


Fig. 19. Normalized stress intensity factor along the crack with different cross-sectional areas of pit

– The effect of pitting corrosion increases with the increase of cross-sectional area of pit. Despite this fact, the comparison between the elliptical and circular cross-sections of pit shows that the radius of elliptical cross-section in the direction of the crack front is one of the significant parameters.

– For a pit with an elliptical cross-section, when the major axis of the ellipse coincides with the direction of the crack face, the effect of pitting corrosion on the SIF reaches a maximum, and this effect gradually decreases with the increase of the angle between the major axis of the ellipse and the direction of the crack face. However, each point along the crack front approximately experiences the same trend.

Література

1. Mahmoud H.N, Dexter R.J. Propagation rate of large cracks in stiffened panels under tension loading. *Marine Structures*. 2005. № 18(3). P. 265–288. DOI: <https://doi.org/10.1016/j.marstruc.2005.09.001>.
2. Yang S., Ni Y.L., Li C.Q. Weight function method to determine stress intensity factor for semi-elliptical crack with high aspect ratio in cylindrical vessels. *Engineering Fracture Mechanics*. 2013. № 109. P. 138–149. DOI: <https://doi.org/10.1016/j.engfracmech.2013.05.014>.
3. Thévenet D., Ghanameh M.F., Zeghloul A. Fatigue strength assessment of tubular welded joints by an alternative structural stress approach. *International Journal of Fatigue*. 2013. № 51. P. 74–82.
4. Fathi A., Aghakouchak A. Prediction of fatigue crack growth rate in welded tubular joints using neural network. *International journal of fatigue*. 2007. № 29(2). P. 261–275. DOI: <https://doi.org/10.1016/j.ijfatigue.2006.03.002>.
5. Lie S.T., Li G., Cen Z. Effect of brace wall thickness and weld size on stress intensity factors for welded tubular T-joints. *Journal of Constructional Steel Research*. 2000. № 53(2). P. 167–182.
6. Huang X., Hancock J.W. The stress intensity factors of semi-elliptical cracks in a tubular welded T-joint under axial loading. *Engineering Fracture Mechanics*. 1988. № 30(1). P. 25–35. DOI: [https://doi.org/10.1016/0013-7944\(88\)90252-4](https://doi.org/10.1016/0013-7944(88)90252-4).
7. Ritchie D., Huijskens H. Fracture mechanics based predictions of the effects of the size of tubular joint test specimens on their fatigue life. *Offshore Mechanics & Arctic Engng. Proc. 8th Intn. Conference*. 1989. Vol. 3. P. 121–127.
8. Olowokere D., Nwosu D. Numerical studies on crack growth in a steel tubular T-joint. *International journal of mechanical sciences*. 1997. № 39(7). P. 859–871. DOI: [https://doi.org/10.1016/S0020-7403\(96\)00087-2](https://doi.org/10.1016/S0020-7403(96)00087-2).
9. Nwosu D., Olowokere D. Evaluation of stress intensity factors for steel tubular T-joints using line spring and shell elements. *Engineering Failure Analysis*. 1995. № 2(1). P. 31–44. DOI: [https://doi.org/10.1016/1350-6307\(95\)00005-B](https://doi.org/10.1016/1350-6307(95)00005-B).
10. Toribio J., Matos J., González B., Escuadra J. Numerical modelling of cracking path in round bars subjected to cyclic tension and bending. *International Journal of Fatigue*. 2014. № 58. P. 20–27. DOI: <https://doi.org/10.1016/j.ijfatigue.2013.03.017>.
11. Qian X., Nguyen C.T., Petchdemanengam Y., Ou Z., Swaddiwudhipong S., Marshall P. Fatigue performance of tubular X-joints with PJP+ welds: II—Numerical investigation. *Journal of Constructional Steel Research*. 2013. № 89. P. 252–261.
12. Dao N.H., Sellami H. Stress intensity factors and fatigue growth of a surface crack in a drill pipe during rotary drilling operation. *Engineering Fracture Mechanics*. 2012. № 96. P. 626–640. DOI: <https://doi.org/10.1016/j.engfracmech.2012.09.025>.
13. Nakai T., Matsushita H., Yamamoto N., editors. Pitting corrosion and its influence on local strength of hull structural members. *ASME 2005 24th International Conference on Offshore Mechanics and Arctic Engineering, American Society of Mechanical Engineers*. Greece. 2005. P. 25–35. DOI: <https://doi.org/10.1115/OMAE2005-67025>.
14. Ji J., Zhang C., Kodikara J., Yang S.Q. Prediction of stress concentration factor of corrosion pits on buried pipes by least squares support vector machine. *Engineering Failure Analysis*. 2015. № 55. P. 131–138.
15. Rahbar-Ranji A., Niamir N., Zarookian A. Ultimate strength of stiffened plates with pitting corrosion. *International Journal of Naval Architecture and Ocean Engineering*. 2015. № 7(3). P. 509–525. DOI: <https://doi.org/10.1515/ijnaoe-2015-0037>.
16. Eslami-majd A., Rahbar-Ranji A. Blast response of corroded steel plates. *Journal of Mechanical Science and Technology*. 2014. № 28(5). P. 1683–1690. DOI: <https://doi.org/10.1007/s12206-014-0313-1>.
17. Eslami-Majd A., Rahbar-Ranji A. Free vibration analysis of corroded steel plates. *Journal of Mechanical Science and Technology*. 2014. № 28(6). P. 2081–2088. DOI: <https://doi.org/10.1007/s12206-013-1114-7>

18. Eslami-Majd A., Rahbar-Ranji A. Deformation behaviour of corroded plates subjected to blast loading. *Journal of Ships and Offshore Structures*. 2015. № 10(1). P. 79–93. DOI: <https://doi.org/10.1080/17445302.2014.889371>.
19. Zhang Y., Huang Y., Zhang Q., Liu G. Ultimate strength of hull structural plate with pitting corrosion damage under combined loading. *Ocean Engineering*. 2016. № 116. P. 273–285.
20. Gandhi P., Murthy D.R., Raghava G., Rao A.M. Fatigue crack growth in stiffened steel tubular joints in seawater environment. *Engineering Structures*. 2000. № 22(10). P. 1390–1401.
21. Xu S-h. Estimating the effects of corrosion pits on the fatigue life of steel plate based on the 3D profile. *International Journal of Fatigue*. 2015. № 72. P. 27–41. DOI: <https://doi.org/10.1016/j.ijfatigue.2014.11.003>.
22. Rokhlin S., Kim J.Y., Nagy H., Zoofan B. Effect of pitting corrosion on fatigue crack initiation and fatigue life. *Engineering Fracture Mechanics*. 1999. № 62(4). P. 425–444. DOI: [https://doi.org/10.1016/S0013-7944\(98\)00101-5](https://doi.org/10.1016/S0013-7944(98)00101-5).
23. Wang W., Zhou A., Robert D., Li C., editors. Assessment of stress intensity factors for cast iron pipes with pitting corrosion. *International conference on Geo-mechanics, Geo-energy and Geo-resources*. 3GDeep Group, Department of Civil Engineering, Monash University. 2016. P. 79–84.
24. Nakai T., Matsushita H., Yamamoto N. Effect of pitting corrosion on local strength of hold frames of bulk carriers (2nd report)—lateral-distortional buckling and local face buckling. *Marine Structures*. 2004. № 17(8). P. 612–641.
25. Jie Z., Li Y., Wei X. A study of fatigue crack growth from artificial corrosion pits at welded joints under complex stress fields. *Fatigue & Fracture of Engineering Materials & Structures*. 2017. № 40(9). P. 1364–1377. DOI: <https://doi.org/10.1111/ffe.12577>.

References

1. Mahmoud, H.N., & Dexter, R.J. (2005). Propagation rate of large cracks in stiffened panels under tension loading. *Marine Structures*, 18(3), 265–288. DOI: <https://doi.org/10.1016/j.marstruc.2005.09.001>.
2. Yang, S., Ni, Y.L., & Li, C.Q. (2013). Weight function method to determine stress intensity factor for semi-elliptical crack with high aspect ratio in cylindrical vessels. *Engineering Fracture Mechanics*, 109, 138–149. DOI: <https://doi.org/10.1016/j.engfracmech.2013.05.014>.
3. Thévenet, D., Ghanameh, M.F., & Zeghloul, A. (2013). Fatigue strength assessment of tubular welded joints by an alternative structural stress approach. *International Journal of Fatigue*, 51, 74–82.
4. Fathi, A., & Aghakouchak A. (2007). Prediction of fatigue crack growth rate in welded tubular joints using neural network. *International journal of fatigue*, 29(2), 261–275. DOI: <https://doi.org/10.1016/j.ijfatigue.2006.03.002>.
5. Lie, S.T., Li, G., & Cen, Z. (2000). Effect of brace wall thickness and weld size on stress intensity factors for welded tubular T-joints. *Journal of Constructional Steel Research*, 53(2), 167–182.
6. Huang, X., & Hancock, J.W. (1988). The stress intensity factors of semi-elliptical cracks in a tubular welded T-joint under axial loading. *Engineering Fracture Mechanics*, 30(1), 25–35. DOI: [https://doi.org/10.1016/0013-7944\(88\)90252-4](https://doi.org/10.1016/0013-7944(88)90252-4).
7. Ritchie, D., & Huijskens, H. (1989). Fracture mechanics based predictions of the effects of the size of tubular joint test specimens on their fatigue life. *Proc. 8th Intn. Conference, Offshore Mechanics & Arctic Engng., Vol. 3*. (pp.121–127).
8. Olowokere, D., & Nwosu, D. (1997). Numerical studies on crack growth in a steel tubular T-joint. *International journal of mechanical sciences*, 39(7), 859–871. DOI: [https://doi.org/10.1016/S0020-7403\(96\)00087-2](https://doi.org/10.1016/S0020-7403(96)00087-2).
9. Nwosu, D., & Olowokere, D. (1995). Evaluation of stress intensity factors for steel tubular T-joints using line spring and shell elements. *Engineering Failure Analysis*, 2(1), 31–44. DOI: [https://doi.org/10.1016/1350-6307\(95\)00005-B](https://doi.org/10.1016/1350-6307(95)00005-B).
10. Toribio, J., Matos, J., González, B., & Escudra, J. (2014). Numerical modelling of cracking path in round bars subjected to cyclic tension and bending. *International Journal of Fatigue*, 58, 20–27. DOI: <https://doi.org/10.1016/j.ijfatigue.2013.03.017>.
11. Qian, X., Nguyen, C.T., Petchdemanengam, Y., Ou, Z., Swaddiwudhipong, S., & Marshall, P. (2013). Fatigue performance of tubular X-joints with PJP+ welds: II—Numerical investigation. *Journal of Constructional Steel Research*, 89, 252–261.

12. Dao, N.H., & Sellami, H. (2012). Stress intensity factors and fatigue growth of a surface crack in a drill pipe during rotary drilling operation. *Engineering Fracture Mechanics*, 96, 626–640. DOI: <https://doi.org/10.1016/j.engfracmech.2012.09.025>.
13. Nakai, T., Matsushita, H., & Yamamoto, N., editors. (2005). Pitting corrosion and its influence on local strength of hull structural members. *ASME 2005 24th International Conference on Offshore Mechanics and Arctic Engineering, American Society of Mechanical Engineers*. Greece. (pp.25–35) DOI: <https://doi.org/10.1115/OMAEE2005-67025>
14. Ji, J., Zhang, C., Kodikara, J., & Yang, S.Q. (2015). Prediction of stress concentration factor of corrosion pits on buried pipes by least squares support vector machine. *Engineering Failure Analysis*, 55, 131–138.
15. Rahbar-Ranji, A., Niamir, N., & Zarookian, A. (2015). Ultimate strength of stiffened plates with pitting corrosion. *International Journal of Naval Architecture and Ocean Engineering*, 7(3), 509–525. DOI: <https://doi.org/10.1515/ijnaoe-2015-0037>.
16. Eslami-majd, A., & Rahbar-Ranji, A. (2014). Blast response of corroded steel plates. *Journal of Mechanical Science and Technology*, 28(5), 1683–1690. DOI: <https://doi.org/10.1007/s12206-014-0313-1>.
17. Eslami-Majd, A., & Rahbar-Ranji, A. (2014). Free vibration analysis of corroded steel plates. *Journal of Mechanical Science and Technology*, 28(6), 2081–2088. DOI: <https://doi.org/10.1007/s12206-013-1114-7>
18. Eslami-Majd, A., & Rahbar-Ranji, A. (2015). Deformation behaviour of corroded plates subjected to blast loading. *Journal of Ships and Offshore Structures*, 10(1), 79–93. DOI: <https://doi.org/10.1080/17445302.2014.889371>.
19. Zhang, Y., Huang, Y., Zhang, Q., & Liu, G. (2016). Ultimate strength of hull structural plate with pitting corrosion damage under combined loading. *Ocean Engineering*, 116, 273–285.
20. Gandhi, P., Murthy, D.R., Raghava, G., & Rao, A.M. (2000). Fatigue crack growth in stiffened steel tubular joints in seawater environment. *Engineering Structures*, 22(10), 1390–1401.
21. Xu, S-h. (2015). Estimating the effects of corrosion pits on the fatigue life of steel plate based on the 3D profile. *International Journal of Fatigue*, 72, 27–41. DOI: <https://doi.org/10.1016/j.ijfatigue.2014.11.003>.
22. Rokhlin, S., Kim, J.Y., Nagy, H., & Zoofan, B. (1999). Effect of pitting corrosion on fatigue crack initiation and fatigue life. *Engineering Fracture Mechanics*, 62(4), 425–444. DOI: 10.1016/S0013-7944(98)00101-5.
23. Wang, W., Zhou, A., Robert, D., & Li, C., editors. (2016). Assessment of stress intensity factors for cast iron pipes with pitting corrosion. *International conference on Geo-mechanics, Geo-energy and Geo-resources. 3GDeep Group, Department of Civil Engineering*. (pp.79–84). Monash University.
24. Nakai, T., Matsushita, H., & Yamamoto, N. (2004). Effect of pitting corrosion on local strength of hold frames of bulk carriers (2nd report)—lateral-distortional buckling and local face buckling. *Marine Structures*, 17(8), 612–641.
25. Jie, Z., Li, Y., & Wei, X. (2017). A study of fatigue crack growth from artificial corrosion pits at welded joints under complex stress fields. *Fatigue & Fracture of Engineering Materials & Structures*, Vol. 40(9), 1364–1377. DOI: <https://doi.org/10.1111/ffe.12577>.

Ahmad Rahbar Ranji, Ахмад Рахбар Ранджи ORCID: <https://orcid.org/0000-0002-7056-929X>

Amirhossein Kaviani, Амирхосейн Кавіані ORCID: <http://orcid.org/0000-0002-2515-6138>

Mehdi Iranmanesh, Мехди Іранманеш

Alireza Dowlatabadi, Аліреза Довлатабади

Received June 06, 2018

Accepted July 07, 2018